This paper is published as part of a *Dalton Transactions* themed issue on:

Thermoelectric Materials

Guest Editor Andrei Shevelkov
Moscow State University, Russia

Published in issue 4, 2010 of *Dalton Transactions*

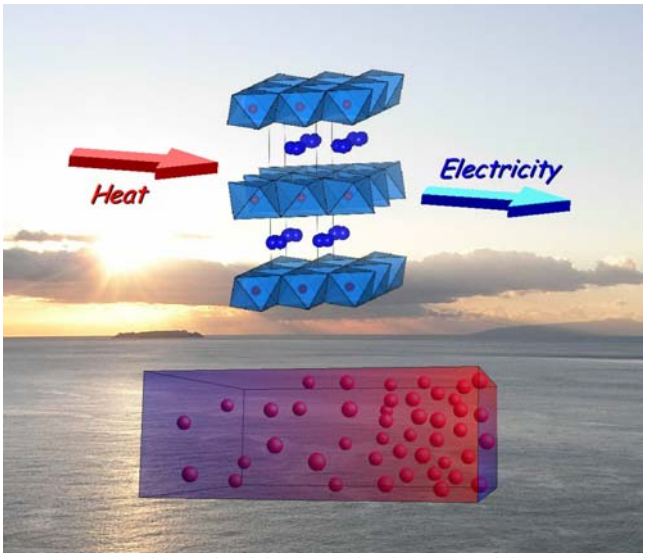

Image reproduced with permission of Ichiro Terasaki

Articles published in this issue include:

PERSPECTIVES:

Thermoelectric clathrates of type I
Mogens Christensen, Simon Johnsen and Bo Brummerstedt Iversen
Dalton Trans., 2010, DOI: 10.1039/b916400f

Wet chemical synthesis and thermoelectric properties of V-VI one- and two-dimensional nanostructures
Genqiang Zhang, Qingxuan Yu and Xiaoguang Li
Dalton Trans., 2010, DOI: 10.1039/b913462j

HOT ARTICLES:

Novel thermoelectric properties of complex transition-metal oxides
Ichiro Terasaki, Manabu Iwakawa, Tomohito Nakano, Akira Tsukuda and Wataru Kobayashi**,**
Dalton Trans., 2010, DOI: 10.1039/b914661j

Effect of Zn doping on improving crystal quality and thermoelectric properties of borosilicides
Takao Mori, David Berthebaud, Toshiyuki Nishimura, Akiko Nomura, Toetsu Shishido and Kazuo Nakajima, *Dalton Trans.,* 2010, DOI: 10.1039/b916028k

Visit the *Dalton Transactions* website for more cutting-edge inorganic and organometallic research
www.rsc.org/dalton

Synthesis, structure, magnetism, and high temperature thermoelectric properties of Ge doped $Yb_{14}MnSb_{11}$†

Japheth F. Rauscher,[a] Catherine A. Cox,[a] Tanghong Yi,[a] Christine M. Beavers,[b] Peter Klavins,[c] Eric S. Toberer,[d] G. Jeffrey Snyder[d] and Susan M. Kauzlarich*[a]

Received 30th September 2009, Accepted 4th November 2009
First published as an Advance Article on the web 30th November 2009
DOI: 10.1039/b920250a

The Zintl phase $Yb_{14}MnSb_{11}$ was successfully doped with Ge utilizing a tin flux technique. The stoichiometry was determined by microprobe analysis to be $Yb_{13.99(14)}Mn_{1.05(5)}Sb_{10.89(16)}Ge_{0.06(3)}$. This was the maximum amount of Ge that could be incorporated into the structure *via* flux synthesis regardless of the amount included in the reaction. Single crystal X-ray diffraction could not unambiguously determine the site occupancy for Ge. Bond lengths varied by about 1% or less, compared with the undoped structure, suggesting that the small amount of Ge dopant does not significantly perturb the structure. Differential scanning calorimetry/thermogravimetry (DSC/TG) show that the doped compound's melting point is greater than 1200 K. The electrical resistivity and magnetism are virtually unchanged from the parent material, suggesting that Yb is present as Yb^{2+} and that the Ge dopant has little effect on the magnetic structure. At 900 K the resistivity and Seebeck coefficient decrease resulting in a zT of 0.45 at 1100 K, significantly lower than the undoped compound.

Introduction

Energy production and consumption is a dominant issue in world news and politics today. World energy consumption is estimated to be ~14 Terawatts per year or about 220 million barrels of oil per day.[1,2] Most of that energy was produced from the burning of hydrocarbons. Much discussion has been made of the side products of the burning of these fuels such as CO_2, CO, and other pollutants but little mention has been made of waste heat. Only about 25% of the fuel energy for a typical internal combustion engine vehicle is utilized in vehicle mobility and accessories. Most energy is lost as heat,[3] and the Department of Energy (DOE) reports a 33–35% efficiency of a typical coal burning power plant. Even the most thermodynamically efficient power generation technologies lose about half of the fuels energy as waste heat and as much as 80% is lost as waste heat in automobiles. Capturing even a small portion of that energy potential could provide as much energy as is currently being produced by nuclear and solar efforts combined.[1-5]

Thermoelectric generators, which have the ability to convert heat energy into electricity, could potentially be used to capture much of the waste heat and convert it into electricity, making power generation more efficient without increasing emissions. Utilizing the Seebeck effect and converting a temperature gradient into a potential difference, these generators are made by combining two thermoelectric materials; one n-type, and one p-type in series.[3-5] Due to their solid state nature, these devices are virtually maintenance free. The reliability of these generators has been established by over 30 years of maintenance free operation in NASA missions such as the Voyager program.[3-5]

In order to take full advantage of the temperature ranges of the waste heat in industrial and automotive applications, segmented thermoelectric generators can be used.[6] In these generators, materials optimized for different temperatures are combined on each of the n and p legs, broadening the operational range that the generator can be effective. Much research has been done on materials for the temperature ranges between room temperature and 600° C, but in order to utilize much of the waste heat mentioned above new materials need to be optimized for the higher temperature range of 800–1000° C as well.

A good thermoelectric generator requires materials that combine three specific properties in the solid. These properties are a high Seebeck (α), low electrical resistivity (ρ) and low thermal conductivity (κ) which combine to form a large figure of merit (zT) in Equation (1), where T is temperature.[7,8] The Seebeck coefficient (α) corresponds to the amount of voltage generated by the material as a consequence of a temperature gradient. Thermal conductivity (κ) is the ability of heat to flow through the solid by conduction.

$$zT = \frac{\alpha^2 T}{\rho\kappa} \quad (1)$$

The lack of a high-quality *p*-type leg material has kept the efficiency of high temperature thermoelectric power generation low. While bulk $Si_{1-x}Ge_x$ alloy with $x \approx 0.3$, has been the state of the art for the high temperature p-type segment of the generator, the zT of 0.6 lowers efficiency for the overall device.[9] Significant

[a]*Department of Chemistry, University of California, One Shields Ave., Davis, CA 95616*
[b]*Advanced Light Source, Lawrence Berkeley National Lab, One Cyclotron Road, Berkeley, CA 94720*
[c]*Department of Physics, University of California, One Shields Ave., Davis, CA 95616*
[d]*California Institute of Technology, 1200 California Blvd., Pasadena, CA 91125*

† Electronic supplementary information (ESI) available: Microprobe of pressed pellets and powder X-ray diffraction data with lattice parameter indexing. X-ray crystallographic data in CIF format for the single-crystal refinements of Ge doped $Yb_{14}MnSb_{11}$. CCDC reference number 752806. For ESI and crystallographic data in CIF or other electronic format see DOI: 10.1039/b920250a

advances in bulk materials have been made with the discovery of the compound $Yb_{14}MnSb_{11}$ which doubles the zT of the p-type $Si_{1-x}Ge_x$ alloy.[10]

$Yb_{14}MnSb_{11}$ is a heavily doped p-type semiconductor with large Seebeck and low thermal conductivity crystallizing in the $Ca_{14}AlSb_{11}$ structure type.[11] The unit cell of the $A_{14}MPn_{11}$ class of compounds contains 208 atoms, shown in Fig. 1, and the asymmetric unit can be described using the Zintl-Klemm formalism as consisting of isolated covalently bonded anions of one $[MPn_4]^{9-}$ tetrahedron, one $[Pn_3]^{7-}$ linear unit, with four Pn^{3-} anions, and 14 A^{2+} cations (A = Ca, Sr, Ba, Yb, Eu; M = Mn, Zn, Al, Ga, In; Pn = P, As, Sb, Bi).[10-27] The valence precise compounds are composed of the alkaline earth cations with M = Al, Ga, In. In the case of M = Zn, Mn, these compounds show unique magnetic and electronic properties and can be formally considered 1 e^- deficient, consistent with the observed p-type electrical conduction. The solid solution $Yb_{14}Mn_{1-x}Zn_xSb_{11}$ with x = 0.4 shows ~10% improved zT at 1275K.[28] The isoelectronic addition of Zn^{2+} for Mn^{2+} has the effect of lowering resistivity without changing the Seebeck coefficient. Similarly, substituting Al for Mn dramatically improves the zT by approximately 30%.[29] The substitution of Al^{3+} for Mn^{2+} adds electrons to this p-type semiconductor and increases the Seebeck coefficient with moderate effect on resistivity. Substitutions on the A site have either been solid solutions of 2+ cations or dopants of 3+ cations such as, Gd for Eu and La for Yb which have produced new magnetic and magnetoresistive properties.[23,26] Substitution of La^{3+} for Yb^{2+} results in a similar enhancement of the zT as that seen for Al, reducing the carrier concentration and increasing Seebeck.[30]

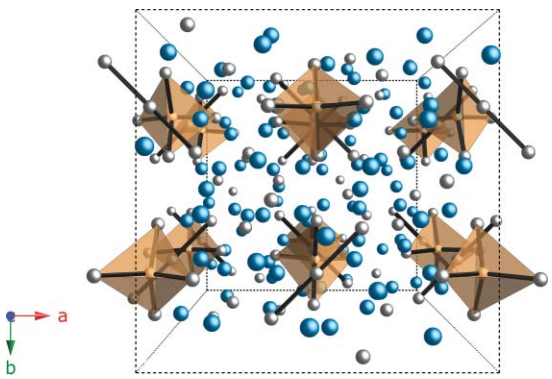

Fig. 1 Crystallographic view of $Yb_{14}MnSb_{11}$ along the c axis. $MnSb_4$ units are indicated by translucent tetrahedral polyhedra. Blue, grey, and brown spheres represent Yb, Sb, and Mn atoms, respectively.

In order to explore further the electronic parameters of this structure type, we initiated a study on elemental substitution of the anion site. Elemental substitution of the anion site may provide an even richer chemistry because of the 4 crystallographic sites available to the anion. The two elements that we have investigated *via* flux synthesis were Te, and Ge. Chemical substitution of either Te or Ge for Sb should change the electron carrier concentration while lowering the lattice thermal conductivity because of the additional structural disorder. This was shown to be the case for Ge doping of the Zintl phase $Yb_{11}Sb_{10}$, $Yb_{11}Sb_{9.3}Ge_{0.5}$,[31] where Ge doping provided lower thermal conductivity without significantly affecting the Seebeck coefficient.

This flux synthesis of the Te and Ge doping for $Yb_{14}MnSb_{11}$ was attempted in order to determine their effect on the high temperature transport properties. Te doping was not successful for the flux reactions investigated. The synthesis, structural characterization, and magnetism along with high temperature thermoelectric property measurements, of the Ge doped phase of $Yb_{14}MnSb_{11}$ is presented and compared to the properties of $Yb_{14}MnSb_{11}$.

Experimental

Synthesis

All materials were handled in an inert atmosphere or under vacuum. Utilizing Sn flux techniques described by Canfield and Fisk,[32-34] Ge doped $Yb_{14}MnSb_{11}$ was obtained by the reaction of the elements in a Sn flux. Sublimed dendritic Yb (Alfa Aesar 99.99%), Te pieces (Alfa Aesar 99.9999%), and Mn chips (Alfa Aesar 99.98%) were cut into small pieces, Sb shot (Alfa Aesar 99.9%), Ge powder (Aldrich 99.999%), and Sn shot (Alfa Aesar 99.99%) were used as received. The elements Yb:Mn:Sb:Ge:Sn were layered in a 5 ml alumina crucible loaded in the molar ratio 14:6:11–x:x:86 (x = 1, 2, 5, 6) scaled to 3 g total reaction mass and sealed in an evacuated quartz tube. The reactants were heated in a programmable furnace to 1373 K over 4 hours then slowly cooled at a rate of 3°/h to 973K. The reaction was allowed to dwell at 973K for 72 hours at which time the molten Sn flux was removed by centrifugation. High yields of large, highly reflective, black crystals were obtained.

Attempts to dope higher amounts of Ge into the $Yb_{14}MnSb_{11}$ structure were made by loading the reactions in the ratios 14:6:11–x:x:86 (x = 7, 8). The reactions were scaled to 3 g of product, sealed in an evacuated quartz tube, and run using the same heating scheme as previously stated. The results were similar dopant levels of Ge as obtained from x = 1-6 reactions but with decreasing quality and yield as x increases. The reaction loaded as 14:6:10:1:86 was deemed most successful for highest yield, and was scaled up to 30 g total weight for full structural and thermoelectric characterization.

Similar reactions were performed for Te doping using the procedure described above; however pristine $Yb_{14}MnSb_{11}$ crystals, as determined by microprobe analysis, were obtained regardless of reaction composition.

Purity was examined using powder X-ray diffraction (XRD) of several ground crystals and thermogravimetry/differential scanning calorimetry (TG/DSC). Microprobe analysis and single crystal X-ray crystallography were used to determine the amount of Ge doped into the structure.

Microprobe

Hot pressed pellets and single crystals were mounted in resin and polished, to ensure no oxidation of the surfaces, before analysis with a Cameca SX-100 electron microprobe equipped with a wavelength-dispersive spectrometer with 20 keV accelerating potential and 10 nA beam current. Pure elemental standards, also polished before analyzed were used to calibrate the net elemental intensities for Yb, Mn, Sb, Ge, and Te. The peaks and background were counted for 10 s for Yb, Mn, Sb, and 30 s for Ge and Te.

Several crystals from each reaction batch were further analyzed by wavelength dispersive spectroscopy (WDS) and 8-15 points were taken on each crystal. SEM and elemental mapping were employed to ensure uniform doping.

Powder X-ray diffraction

X-ray powder diffraction data were collected for Ge doped $Yb_{14}MnSb_{11}$ with either an INEL CPS 120 over 0–120° 2θ at 10° incident angle operating with Co K_α (1.78897 Å) radiation or a Bruker D8 Advance diffractometer operating at 40 kV and 40 mA with Cu K_α radiation (1.54056 Å) with a 0.016 step size and 1.9 s/step over 2–80° 2θ. Data acquisition was performed with software supplied with the instruments, analysis and refinement for lattice parameters was performed using MDI JADE 6.1.[35] Whole pattern fitting and Rietveld refinement were performed with Pseudo-Voigt as profile shape function, $Yb_{14}MnSb_{11}$ positional parameters from Chan *et al.*, and considering the contribution of Cu $K\alpha_2$.[13,35,36] The diffraction patterns from various samples were also compared to those calculated from the single crystal data using the JPOWD 5.1 and Crystal Maker 7.1.[13]

Single crystal X-ray diffraction

Intensity data were collected at 90 K using a Bruker SMART 1000 CCD diffractometer utilizing a graphite-monochromatic Mo K_α radiation (λ = 0.71069 Å) on a silvery crystal with dimensions of 0.098 × 0.132 × 0.058 mm. A full sphere of data was collected with an exposure time of 25 s per frame, 0.3° ω-scans. The SMART software was used for data acquisition, and SAINT was used to correct for Lorentz and polarization effects. The data were corrected for absorption effects utilizing the multi-scan technique of the SADABS program. The structure solution was obtained by direct methods and refined on a full matrix by a least squares refinement using the SHELXTL 5.10 package.

An additional data set was collected at the Advanced Light Source in Berkeley, CA on another crystal in order to minimize absorption and identify the possibility of site preference for Ge in this structure. A metallic shard of dimensions 0.07 × 0.05 × 0.02 mm^3 was mounted in the 90(2) K nitrogen cold stream provided by an Oxford Cryosystems Cryostream on the goniometer head of a Bruker D8 diffractometer equipped with an ApexII CCD detector, on beamline 11.3.1. Diffraction data were collected using synchrotron radiation monochromated with silicon(111) to a wavelength of 0.77490 Å. An approximate full sphere of data to 2θ = 67° was collected using 0.3° ω scans. A multi-scan absorption correction was applied using the program SADABS-2008/1.[37] A total of 40947 reflections were collected, of which 2302 were unique [R(int) = 0.0857] and 2280 were observed [I>2σ (I)]. The structure was solved by direct methods (SHELXS) and refined by full-matrix least-squares on F^2 (SHELXL97) using 61 parameters. The formula given in the CIF is the formula from microprobe analysis. It was not possible to refine meaningful shared Ge sites however, so Ge was omitted from the final model. The maximum and minimum peaks in the final difference Fourier map were 1.923 and –2.814 $eÅ^{-3}$. Crystal data: $Yb_{13.99}MnSb_{10.89}Ge_{0.06}$, Mw= 3806.06, tetragonal, $I4_1/acd$, a = 16.578(2) Å, c = 21.897(3) Å, V = 6018.2(15) $Å^3$, T = 90(2) K, Z = 8, R1 [I>2σ (I)] = 0.0287, wR_2 (all data) = 0.0731, GOF (on F^2) = 1.099. Data collection and refinement are summarized in Table 1.

Table 1 Selected data from the single-crystal structure refinement of Ge doped $Yb_{14}MnSb_{11}$

Parameter	
Empirical Formula[a]	$Yb_{13.99(14)}Mn_{1.05(5)}Sb_{10.89(16)}Ge_{0.06(3)}$
Crystal Dimensions (mm)	0.07 × 0.05 × 0.02
Wavelength (Å)	0.77490
Space Group	$I4_1/acd$
Z	8
Temp (K)	90(2)
a (Å)	16.578(2)
c (Å)	21.897(3)
Cell Volume ($Å^3$)	6018.2(15)
θ range	6.32° <2θ<67.22°
No. of collected reflections	40947
No. of unique reflections	2302
ρ_{calc} (g cm^{-3})	8.402
μ Mo Kα (mm^{-1})	65.868
R1 [I > 2σ(I)][b]	0.0287
wR2[c]	0.0722
Largest diff peak and hole (e $Å^{-3}$)	1.923 and –2.814

[a] Formula from microprobe. [b] $R1 = [\sum||F_o| - |F_c||]/\sum|F_o|$. [c] $wR2 = [\sigma^2(F_o) + (0.0471P)^2 + (0.5945P)]$ where $P = [\max(F_o^2,0) + 2F_c^2/3]$.

Thermogravimetry and differential scanning calorimetry (TG/DSC)

A Netzsch Thermal Analysis STA 409 cell equipped with a TASC 414/2 controller and PU 1.851.01 power unit was used to evaluate the thermal properties of the Ge doped $Yb_{14}MnSb_{11}$ between 298 and 1373 K. After a baseline was established, finely ground powder from single crystals (~25 mg) or a shard of a hot pressed pellet (~50 mg) were placed into Al_2O_3 crucibles and heated under an Ar flow at 10 K/min with an acquisition rate of 10 data points/K.

Magnetization and magnetoresistance measurements

Direct current magnetization data were obtained with a Quantum Design Magnetic Property Measurement System (MPMS) Superconducting Quantum Interference Device (SQUID) magnetometer with a 7 T superconducting magnet. The temperature-dependant magnetization data were obtained by first measuring the zero field cooled magnetization while warming from 5 K to 300 K, then measuring magnetization while cooling back to 5 K with the field applied to obtain the field cooled data. Field-dependant magnetization data were taken at 5 K with H swept from 0 T to 5 T to −5 T and back to 0 T. The single crystal that was used for structure determination was oriented with the *c* axis parallel and perpendicular to H while mounted in a low background holder. Magnetoresistance measurements were performed on a block shaped crystal with dimensions of 0.49 × 0.61 × 0.11 mm from the same batch of sample using standard four-probe method with an applied current of 1 mA along the *c* axis on the 2 outer leads (Keithley model 224 current source) and the voltage was measured along the 2 inner leads (Keithley model 181 nanovoltmeter).

Thermoelectric properties sample preparation

Several large samples (~8 g each) of single crystals were synthesized and ball milled to fine powder. The finely ground polycrystalline powder (~8 g) was hot pressed in high-density graphite dies and a cylinder of 12 mm in diameter was obtained. Experimental density (calculated from measured dimensions and weight) was found to be 8.43 g/cm^3, 99.7% of the theoretical density. Hot-pressing was conducted at 126 MPa and 1173 K for 1 h under argon. For electrical and thermal transport properties and Seebeck coefficient measurements, disks (typically 1 mm thick and 12 mm diameter slice) were cut from the cylinder using a diamond saw. All physical properties were measured between room temperature and 1173 K on at least two independently prepared samples.

Resistivity measurements and hall effect

The electrical resistivity (ρ) was measured using the van der Pauw technique with a current of 100 mA and a special high-temperature apparatus.[38] The Hall coefficient was measured in the same apparatus with a forward and reverse magnetic field value of ~9500 G. The carrier density (n) was calculated from the Hall coefficient (R_H) assuming a scattering factor of 1.0 in a single-carrier scheme, with $n = 1/R_H e$, where n is the densities of charge carriers (holes) and e the charge of the electron. The Hall mobility (μ_H) was calculated from the Hall coefficient and resistivity values with $\mu_H = R_H/\rho$.

Thermal conductivity measurements

The thermal diffusivities were measured for several samples using a flash diffusivity technique (LFA457, NETSZCH).[39] The previously measured heat capacity for $Yb_{14}MnSb_{11}$ was used.[40] The thermal conductivity (κ) was calculated from the measured heat capacity, experimental density, and experimental thermal diffusivity values.

Seebeck measurements

The Seebeck coefficient (α) was measured using a high-temperature light pulse technique using W/Nb thermocouples.[41]

Results and discussion

Synthesis and structure

The Sn flux route to single crystals of $Yb_{14}MnSb_{11}$ has been described previously.[15] In order to dope Ge into the structure, the relative amount of Ge and Sb were varied so that the total reflected the stoichiometry of 11 for the expected amount of anion, if the sites were fully occupied in $Yb_{14}MnSb_{11}$. This strategy had been shown to be successful in both the cation and metal doping of this structure.[28-30,40] Attempts to prepare the Te doped crystals following the same flux procedure were not successful and resulted in pristine $Yb_{14}MnSb_{11}$ and no further discussion for those investigations will be presented. The Ge doped $Yb_{14}MnSb_{11}$ could be prepared, however only a small amount of Ge was incorporated and regardless of the initial flux ratios investigated, the composition remained the same.

Electron microprobe analysis was performed on both the single crystals and pressed pellets. The backscattered electron microscopy (BSE) image and element mapping shown in Fig. 2 indicate that the crystals were homogeneous. The composition across several crystals prepared *via* independent reactions was determined to be $Yb_{13.99(14)}Mn_{1.05(5)}Sb_{10.89(16)}Ge_{0.06(3)}$ with standard deviations provided in parentheses. The compositions were the same within error for all samples prepared with various amounts of Ge, suggesting that this is the limit by flux synthesis, although it is possible that higher concentrations may be possible *via* careful powder metallurgical routes. The Ge content is low, but above the detection threshold. A few of the large crystals showed inclusions of Sn (ESI†), however there was no evidence for Sn substitution in the structure. The pellets used for high temperature transport and thermal diffusivity measurements were also characterized *via* microprobe analysis and provided the same composition. Microprobe analysis of the Ge doped crystals and pellets indicated a thin oxide coating when left in air for several days that could be removed by polishing.

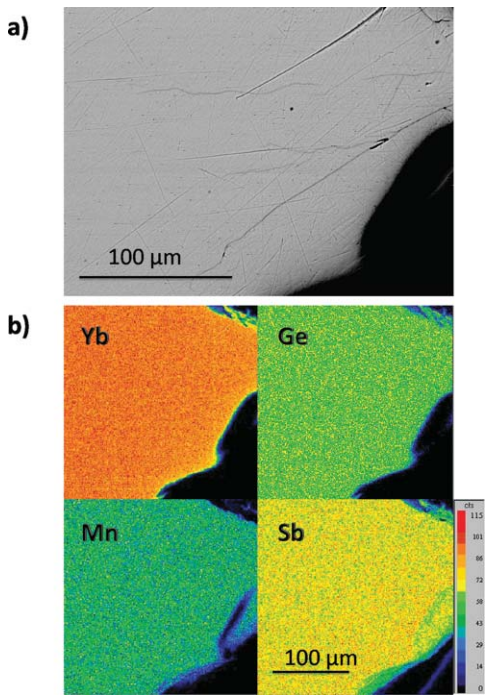

Fig. 2 a) Backscattered electron microscopy image of a Ge doped $Yb_{14}MnSb_{11}$ crystal, b) elemental maps showing homogeneous distribution of elements across a crystal.

The X-ray powder diffraction pattern of the Ge doped sample shows the sample to be single phase as there was no evidence for unindexed peaks (ESI†). The X-ray diffraction data after hot pressing were similar suggesting no impurities or at least less than a few weight percent. The lattice parameters from room temperature powder diffraction for both $Yb_{14}MnSb_{11}$ and the Ge doped phase prepared *via* flux synthesis were determined. $Yb_{14}MnSb_{11}$ provided the following lattice parameters: $a = b = 16.617$ (1), $c = 21.999$ (1) Å. Ge doped $Yb_{14}MnSb_{11}$ provided slightly smaller lattice parameters with $a = b = 16.610$ (1) and $c = 21.986$ (1) Å. The refinement parameters were similar with R = 4.40% and 4.54% for the pristine and doped samples, respectively.

The structure was characterized by single crystal X-ray diffraction and data collection and refinement parameters are provided

Table 2 Selected bond distances and angles of Ge doped $Yb_{14}MnSb_{11}$ compared with pristine $Yb_{14}MnSb_{11}$[13]

Bond	$Yb_{14}MnSb_{11}$	Ge Doped	Difference
Sb(1)-Sb(4)	3.195(1)	3.1842(8)	0.011(1)
Sb(1)-Yb(1) × 2	3.204(1)	3.1956(6)	0.008(1)
Sb(1)-Yb(2) × 2	3.284(1)	3.2767(6)	0.007(1)
Sb(1)-Yb(3)	3.338(1)	3.3314(5)	0.007(1)
Sb(1)-Yb(4)	3.171(1)	3.1666(5)	0.004(1)
Sb(2)-Mn × 4	2.750(1)	2.7418(6)	0.008(1)
Sb(2)-Yb(1)	3.155(1)	3.1486(7)	0.006(1)
Sb(2)-Yb(1′)	3.180(1)	3.1775(7)	0.002(1)
Sb(2)-Yb(2)	3.745(1)	3.7387(8)	0.006(1)
Sb(2)-Yb(2′)	3.139(1)	3.1328(7)	0.006(1)
Sb(2)-Yb(3)	3.226(1)	3.2190(7)	0.007(1)
Sb(2)-Yb(4)	3.159(1)	3.1535(7)	0.005(1)
Sb(2)-Yb(4′)	3.394(1)	3.3838(7)	0.010(1)
Sb(3)-Yb(1)	3.175(1)	3.1669(7)	0.008(1)
Sb(3)-Yb(1′)	3.194(1)	3.1938(7)	0.000(1)
Sb(3)-Yb(2)	3.167(1)	3.1580(7)	0.009(1)
Sb(3)-Yb(2′)	3.274(1)	3.2665(7)	0.007(1)
Sb(3)-Yb(3)	3.134(1)	3.1265(7)	0.007(1)
Sb(3)-Yb(4)	3.212(1)	3.2056(7)	0.006(1)
Sb(3)-Yb(4′)	3.194(1)	3.1850(7)	0.009(1)
Sb(3)-Yb(4″)	3.709(1)	3.6987(8)	0.010(1)
Sb(4)-Yb(1) × 4	3.181(1)	3.1744(5)	0.007(1)
Sb(4)-Yb(2) × 4	3.423(1)	3.4165(5)	0.006(1)
Sb(2)-M-Sb(2′)	105.61(2)	105.563(11)	0.05(2)
Sb(2)-M-Sb(2″)	117.50(4)	117.61(2)	-0.11(4)

in Table 1. Important bond distances and angles are provided in Table 2 and the percent change compared to $Yb_{14}MnSb_{11}$ is provided. The largest differences in bond length are about 1%; therefore, the small amount of Ge dopant does not significantly change the structure. Two data sets and refinements, one on a conventional X-ray source and one with synchrotron radiation were obtained and the results were similar. Only the synchrotron data and refinement are provided, as that data provides the minimum absorption errors. Similar to our results for doping Ge into $Yb_{11}Sb_{10}$,[31] $Yb_{14}MnSb_{11}$ only incorporates a small amount of Ge into the unit cell when prepared from a Sn flux.[31] However, unlike in the $Yb_{11}Sb_{10}$ case, the Ge would not satisfactorily refine on the Sb site.

$Yb_{14}MnSb_{11}$ crystallizes in the $Ca_{14}AlSb_{11}$ structure type (Fig. 1) and has been described in detail previously.[13,24,42-44] The structure consists of 4 crystallographic sites for the cation and anion, in this case, Yb and Sb, whereas the metal, Mn, is described by one crystallographic site. The initial structure was refined as $Yb_{14}MnSb_{11}$. Several models were employed to determine where Ge might reside in this structure. Since Ge doped into $Yb_{11}Sb_{10}$ on the Sb site, a model in which Ge was placed on the Sb sites was refined. However, the occupancy of Ge on all the Sb sites quickly went to zero. Ge was also refined as the central metalloid in the $MnSb_4$ tetrahedron, and on all four of the Yb sites. In the case of the Ge on the Mn site, the refinement was unstable. The refinement of Ge on the Yb sites was stable, but after many refinement cycles, the Ge occupancy went to zero. Therefore, the final refinement does not include Ge.

Cation site preference in this structure type has been observed for the isostructural compound $Eu_{14}MnSb_{11}$, where Yb, Ca, Sr, and Ba replaced Eu.[45] The site preference was attributed to cation size and matrix effects, however the amount of site substitution was significantly higher than in this example.[45]

Germanium is not always a predictable element as it can occupy many different oxidation states. In Zintl phases with electronegative group 15 elements such as nitrogen, Ge can be assigned oxidation states from +4 to -4.[46] In clathrate structures such as $Ba_8Ga_{16}Ge_{30}$, Ge is formally considered to be zero valent.[47] In the only example of a phase in the Yb-Ge-Sb ternary phase diagram, $Yb_8Ge_3Sb_5$, Ge shows only homoatomic bonds to form infinite chains of edge-shared tetrahedra.[48,49] The fact that bond distances are not changing significantly in this structure, and the fact that the amount of Ge is small, leads to problems assigning site preference for Ge in this structure.

Properties measurements

Thermal behavior was investigated *via* TG/DSC. Fig. 3 shows the data for both the hot pressed and single crystal samples, indicating that the material is stable to 1273 K under flowing argon. The single crystal shows much larger effects than the powder sample presumably due to surface interaction and wetting of the crucible. The continual minor increase in the DSC data seen in the powder sample as a function of increasing temperature with no weight loss or gain is consistent with sintering during the heating process and is also consistent with the powder X-ray diffraction data indicating that the sample is phase pure. A small amount of residual tin flux is present in the single crystal sample according to the small endotherm at ~505 K, the melting point of tin. No Sn signature was observed in the hot pressed pellet suggesting that the small amount of Sn is removed during the hot press process. The TG data show that there is no weight loss or gain throughout the temperature range consistent with no loss of Yb, Sb, Mn or Ge from the compound and also no oxidation occurring during the measurement.

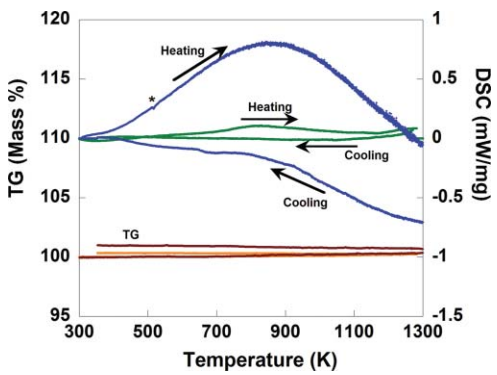

Fig. 3 Thermogravimetry/differential scanning calorimetry (TG/DSC) under flowing argon of a single crystal (thick blue and brown curves are DSC and TG data, respectively) and hot-pressed pellet (thin green and orange curves are DSC and TG data, respectively). DSC data are indicated as heating or cooling curves and TG curves are identified. * indicates melting point of tin.

Magnetism

The ferromagnetic ordering temperature and magnetic moment is consistent with what has been previously published for the undoped $Yb_{14}MnSb_{11}$. Fig. 4 shows the hysteresis measurement aligned for the maximum moment, consistent with 4 unpaired spins. The small amount of Ge has little effect on the magnetic

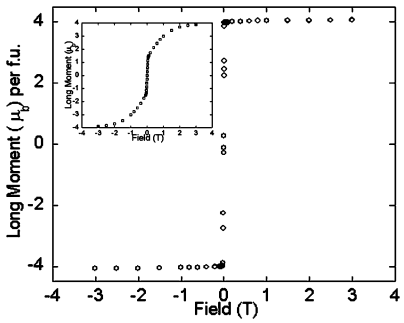

Fig. 4 Hysteresis *versus* applied field at T = 5 K for a single crystal of Ge doped $Yb_{14}MnSb_{11}$ with both hard (inset) and soft axis measurement aligned for the maximum moment.

moment or ordering temperature. This is quite different from the cation doped $Yb_{14}MnSb_{11}$ (La, Gd) where small amounts of the dopants made significant effects reflected in the magnetic data.[23,26] Fig. 5 shows the magnetization *vs.* temperature and the inverse susceptibility (inset) for the Ge doped compound. Single crystal resistivity *vs.* temperature is also shown in Fig. 5. The room temperature resistivity value is 2.14 mΩ cm, slightly higher than that reported for $Yb_{14}MnSb_{11}$. The inset shows the hysteresis measurement aligned for the maximum moment, consistent with 4 unpaired spins.

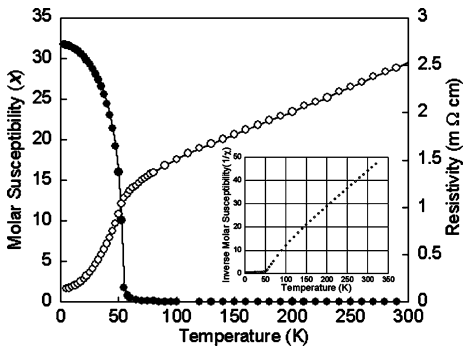

Fig. 5 Temperature dependant resistivity (open circles), molar susceptibility (filled circles) and the inverse molar susceptibility (inset) of a single crystal of Ge doped $Yb_{14}MnSb_{11}$.

Thermoelectric property measurements

Hot pressed pellets were used to measure the electrical properties of Ge doped $Yb_{14}MnSb_{11}$ and compared with published data for $Yb_{14}MnSb_{11}$.[10,40] Temperature dependant resistivity data presented in Fig. 6 shows resistivity increases with increasing temperature from 2.54 mΩ cm at room temperature to 4.23 mΩ cm at ~1065 K. The data reveals a larger residual term following Ge-doping, similar to that observed for the low temperature single crystal measurement. The slope of the resistivity of the Ge doped sample is suppressed compared to the pristine compound. The small hysteresis in the resistivity present in both samples at different temperatures (T ~ 900 K for Ge doped and ~950 °C for pristine sample) may indicate the presence of a small amount of impurity phase, not apparent in the X-ray powder diffraction pattern. Hall effect measurements show nearly identical *n* at moderate temperatures, as expected for the small amount of

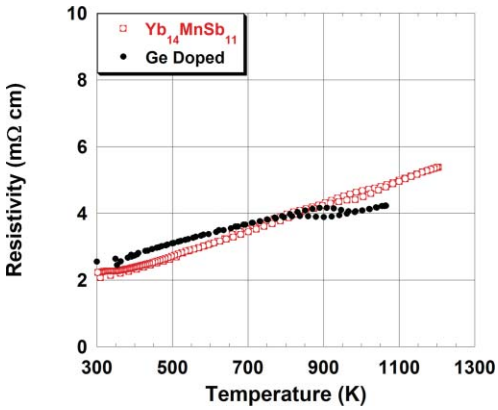

Fig. 6 High temperature resistivity data for $Yb_{14}MnSb_{11}$ and Ge doped $Yb_{14}MnSb_{11}$. Black filled circle is Ge doped, open red square is pristine $Yb_{14}MnSb_{11}$.

doping of Ge, and consistent with the low temperature resistivity and magnetism.

Seebeck, total thermal conductivity, and figure of merit zT for $Yb_{14}MnSb_{11}$ and Ge doped $Yb_{14}MnSb_{11}$ is shown in Fig. 7. Both $Yb_{14}MnSb_{11}$ and Ge doped $Yb_{14}MnSb_{11}$ display p-type Seebeck values that increase with temperature. The doped compound increases from ~55 μV/K at room temperature to ~148 μV/K at 1120 K which is lower than that for the pristine material. These differences in high temperature transport properties could result from a reduction in the band gap or the presence of an impurity phase not apparent in either the powder X-ray diffraction or microprobe analysis. The valence band edge in this structure type is dominated by the $MnSb_4$ tetrahedra[17] and Ge doping would lead to an alteration of states near the valence band edge and hence a decreased band gap. Fig. 7b shows that the thermal conductivity is low in these samples 0.98 W/m K at room temperature and increases with increasing temperature to 1.19 W/m K at 1200 K. The zT value is lower than the parent material (Fig. 7c) reaching $zT = 0.45$ while the previously published pristine compound has $zT = 0.70$ at 1100 K.[10,40]

Summary

A limited amount of Ge has been shown to dope into $Yb_{14}MnSb_{11}$ *via* Sn flux synthesis. Single crystal X-ray diffraction indicated that Ge doping does not significantly change the structure and any site preference of Ge cannot be unambiguously determined. Magnetic behavior and low temperature resistivity are virtually unchanged with respect to $Yb_{14}MnSb_{11}$, consistent with Yb being Yb^{2+}. While there is initial lowering of the thermal conductivity at low temperature, above 500 K the Seebeck coefficients are significantly diminished. Thermal conductivity is compensated at high temperatures providing the lower zT for the Ge doped compound. Doping with a small amount of Ge changes the high temperature properties so that zT is diminished compared with the parent compound. Doping with other elements within the group 15 column may provide a better direction to further optimize this material to enhance the high zT.

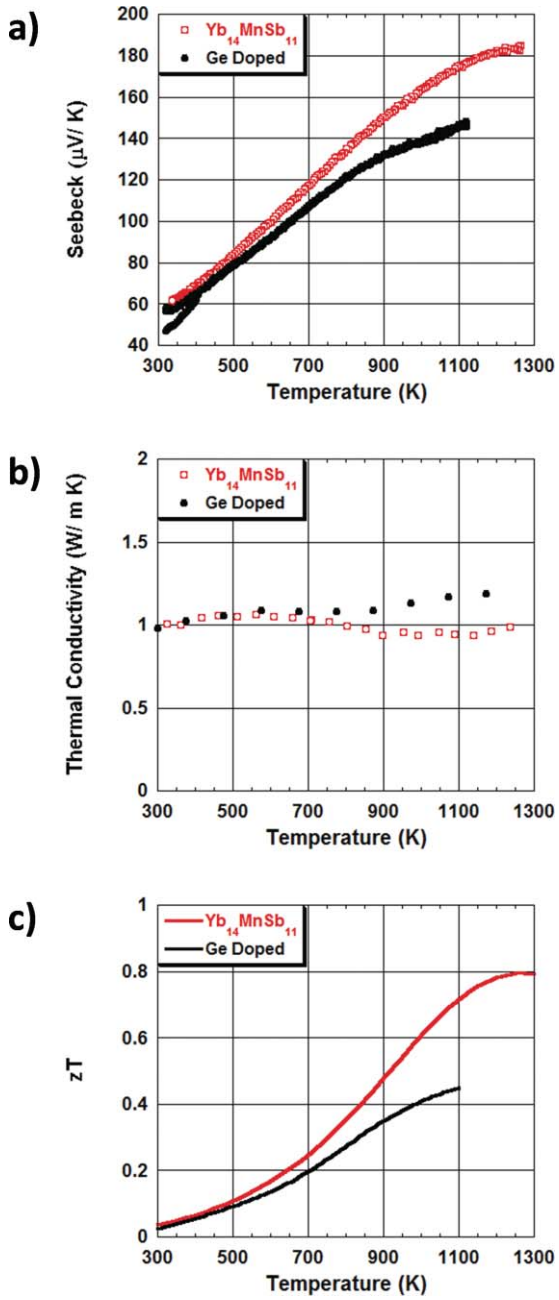

Fig. 7 a) Seebeck, b) total thermal conductivity, (black filled circle is Ge doped, open red square is pristine $Yb_{14}MnSb_{11}$) and c) figure of merit zT curves for $Yb_{14}MnSb_{11}$ (red) and Ge doped $Yb_{14}MnSb_{11}$ (black).

Acknowledgements

We thank Marilyn Olmstead for assistance with crystallography and Sarah Roeske for assistance with microprobe analysis. Portions of this work were carried out at the Jet Propulsion Laboratory, California Institute of Technology, under contract with NASA. This research was funded by NSF DMR-0600742 and the Beckman Foundation at Caltech.

References

1 A. Slaoui and R. T. Collins, *MRS Bull.*, 2007, **32**, 211–218.
2 R. E. Smalley, *MRS Bull.*, 2005, **30**, 412–417.
3 J. Yang, Potential Applications of Thermoelectric Waste Heat Recovery in the Automotive Industry. In *2005 International Conference on Thermoelectrics*, 2005.
4 T. M. Tritt, *Science*, 1996, **272**, 1276–1277.
5 T. M. Tritt and M. A. Subramanian, *MRS Bull.*, 2006, **31**, 188–194.
6 G. J. Snyder, *Appl. Phys. Lett.*, 2004, **84**, 2436–2438.
7 F. J. DiSalvo, *Science*, 1999, **285**, 703–706.
8 *Thermoelectrics Handbook: Macro to Nano*, CRC Press, Boca Raton, FL, 2006.
9 C. B. Vining, in *CRC Handbook of Thermoelectrics*, ed. M. Rowe, CRC, Boca Raton, 1995, pp. 329–337.
10 S. R. Brown, S. M. Kauzlarich, F. Gascoin and G. J. Snyder, *Chem. Mater.*, 2006, **18**, 1873–1877.
11 G. Cordier, H. Schäfer and M. Stelter, *Z. Anorg. Allg. Chem.*, 1984, **519**, 183–188.
12 K. S. Burch, A. Schafgans, N. P. Butch, T. A. Sayles, M. B. Maple, B. C. Sales, D. Mandrus and D. N. Basov, *Phys. Rev. Lett.*, 2005, **95**, 046401.
13 J. Y. Chan, M. M. Olmstead, S. M. Kauzlarich and D. J. Webb, *Chem. Mater.*, 1998, **10**, 3583–3588.
14 I. R. Fisher, S. L. Bud'ko, C. Song, P. C. Canfield, T. C. Ozawa and S. M. Kauzlarich, *Phys. Rev. Lett.*, 2000, **85**, 1120–1123.
15 I. R. Fisher, T. A. Wiener, S. L. Bud'ko, P. C. Canfield, J. Y. Chan and S. M. Kauzlarich, *Phys. Rev. B: Condens. Matter Mater. Phys.*, 1999, **59**, 13829–13834.
16 R. F. Gallup, C. Y. Fong and S. M. Kauzlarich, *Inorg. Chem.*, 1992, **31**, 115–118.
17 A. P. Holm, S. M. Kauzlarich, S. A. Morton, G. D. Waddill, W. E. Pickett and J. G. Tobin, *J. Am. Chem. Soc.*, 2002, **124**, 9894–9898.
18 A. P. Holm, T. C. Ozawa, S. M. Kauzlarich, S. A. Morton, G. D. Waddill and J. G. Tobin, *J. Solid State Chem.*, 2005, **178**, 262–269.
19 S. M. Kauzlarich, *Comments Inorg. Chem.*, 1990, **10**, 75.
20 S. M. Kauzlarich, A. C. Payne and D. J. Webb, in *Magnetism: Molecules to Materials III*, eds. J. S. Miller and M. Drillon, Wiley-VCH, Weinham, Editon edn., 2002, pp. 37-62.
21 *Chemistry, Structure, and Bonding of Zintl Phases and Ions*, ed. S. M. Kauzlarich, VCH Publishers, Inc, New York, 1996.
22 S. M. Kauzlarich, S. R. Brown and G. J. Snyder, *Dalton Trans.*, 2007, 2099–2107.
23 S. M. Kauzlarich, P. Klavins, J. Z. Liu, R. N. Shelton and D. J. Webb, *Phys. Rev. B: Condens. Matter Mater. Phys.*, 2000, **61**, 459–463.
24 A. Rehr, T. Y. Kuromoto, S. M. Kauzlarich, J. Delcastillo and D. J. Webb, *Chem. Mater.*, 1994, **6**, 93–99.
25 R. A. Ribeiro, Y. Hadano, S. Narazu, K. Suekuni, M. A. Avila and T. Takabatake, *J. Phys.: Condens. Matter*, 2007, **19**, 376211.
26 B. C. Sales, P. Khalifah, T. P. Enck, E. J. Nagler, R. E. Sykora, R. Jin and D. Mandrus, *Phys. Rev. B: Condens. Matter Mater. Phys.*, 2005, **72**, 205207.
27 D. Sánchez-Portal, R. M. Martin, S. M. Kauzlarich and W. E. Pickett, *Phys. Rev. B: Condens. Matter Mater. Phys.*, 2002, **65**, 144414.
28 S. R. Brown, E. S. Toberer, T. Ikeda, C. A. Cox, F. Gascoin, S. M. Kauzlarich and G. J. Snyder, *Chem. Mater.*, 2008, **20**, 3412–3419.
29 E. S. Toberer, C. A. Cox, S. R. Brown, T. Ikeda, A. F. May, S. M. Kauzlarich and G. J. Snyder, *Adv. Funct. Mater.*, 2008, **18**, 2795–2800.
30 E. S. Toberer, S. R. Brown, T. Ikeda, S. M. Kauzlarich and G. J. Snyder, *Appl. Phys. Lett.*, 2008, **93**, 062110.
31 J. F. Rauscher, S. M. Kauzlarich, T. Ikeda and G. J. Snyder, *Z. Anorg. Allg. Chem.*, 2007, **633**, 1587–1594.
32 M. G. Kanatzidis, R. Pottgen and W. Jeitschko, *Angew. Chem., Int. Ed.*, 2005, **44**, 6996–7023.
33 P. C. Canfield and I. R. Fisher, *J. Cryst. Growth*, 2001, **225**, 155–161.
34 P. C. Canfield and Z. Fisk, *Philosophical Magazine B: Physics of Condensed Matter: Statistical Mechanics, Electronic, Optical and Magnetic Properties*, 1992, **65**, 1117–1123.
35 *MDI, Materials Data*, Livermore, CA, 2003.
36 *Inorganic Crystal Structure Database, National Institute of Standards and Technology Version 1.3.3*, 2004.
37 G. M. Sheldrick, *Acta Crystallogr., Sect. A: Found. Crystallogr.*, 2008, **64**, 112–122.
38 J. A. McCormack and J. P. Fleurial, *Materials Research Society Symposium Proceedings*, 1991, **234**, 135–143.
39 J. W. Vandersande, C. Wood, A. Zoltan and D. Whittenberger, *Thermal Conductivity*, 1988, **19**, 445–452.
40 C. A. Cox, E. S. Toberer, A. A. Levchenko, S. R. Brown, G. J. Snyder, A. Navrotsky and S. M. Kauzlarich, *Chem. Mater.*, 2009, **21**, 1354–1360.

41 C. Wood, D. Zoltan and G. Stapfer, *Rev. Sci. Instrum.*, 1985, **56**, 719–722.
42 J. Y. Chan, M. E. Wang, A. Rehr, S. M. Kauzlarich and D. J. Webb, *Chem. Mater.*, 1997, **9**, 2131–2138.
43 T. Y. Kuromoto, S. M. Kauzlarich and D. J. Webb, *Chem. Mater.*, 1992, **4**, 435–440.
44 A. Rehr and S. M. Kauzlarich, *J. Alloys Compd.*, 1994, **207–208**, 424–426.
45 H. Kim, P. Klavins and S. M. Kauzlarich, *Chem. Mater.*, 2002, **14**, 2308–2316.
46 S. J. Clarke and F. J. DiSalvo, *Inorg. Chem.*, 2000, **39**, 2631–2634.
47 M. Christensen and B. B. Iversen, *Chem. Mater.*, 2007, **19**, 4896–4905.
48 S. Margadonna, K. Prassides, M. Chondroudi, J. R. Salvador and M. G. Kanatzidis, *Chem. Commun.*, 2005, 5754–5756.
49 J. R. Salvador, D. Bilc, S. D. Mahanti, T. Hogan, F. Guo and M. G. Kanatzidis, *J. Am. Chem. Soc.*, 2004, **126**, 4474–4475.

